Available online at www.sciencedirect.com

ScienceDirect

Transportation Research Procedia 35 (2018) 44–53

Transportation Research Procedia

www.elsevier.com/locate/procedia

International Conference on Air Transport – INAIR 2018

An Innovative Algorithm to Estimate Risk Optimum Path for Unmanned Aerial Vehicles in Urban Environments

Stefano Primatesta[a], Luca Spanò Cuomo[b], Giorgio Guglieri[b,*], Alessandro Rizzo[c]

[a]*Politecnico di Torino, Dipartimento di Automatica e Informatica, Corso Duca degli Abruzzi 24, 10129 Torino, Italy*
[b]*Politecnico di Torino, Dipartimento di Ingegneria Meccanica e Aerospaziale, Corso Duca degli Abruzzi 24, 10129 Torino, Italy*
[c]*Politecnico di Torino, Dipartimento di Elettronica e Telecomunicazioni, Corso Duca degli Abruzzi 24, 10129 Torino, Italy*

Abstract

The diffusion of the Unmanned Aerial Vehicles (UAVs) requires a suitable approach to define safe flight operations. In this paper, an innovative algorithm able to quantify the risk to the population and to search for the minimum risk path is proposed. The method has two main phases: in the former, a risk-map is generated quantifying the risk of a specific area, in the latter, a path planning algorithm seeks for the optimal path minimizing the risk. The risk-map is generated with a risk assessment method combining layers related to the population density, the sheltering factor, no-fly zones and obstacles. The risk-aware path planning is based on the well-known Optimal Rapidly-exploring Random Tree, with the minimization of the risk cost with respect to the flight time. Simulation results corroborate the validity of the approach.

© 2018 The Authors. Published by Elsevier B.V.
This is an open access article under the CC BY-NC-ND license (https://creativecommons.org/licenses/by-nc-nd/4.0/)
Selection and peer-review under responsibility of the scientific committee of the International Conference on Air Transport – INAIR 2018.

Keywords: unmanned aerial vehicles; risk map; risk assessment; risk-aware path planning; RRT*;

1. Introduction

The presence of UAVs in our life is growing up and their extensive use has induced the rapid growth of the related research area. They are used in a wide variety of applications, such as surveillance, search and rescue and mapping, as discussed by Chmaj and Selvaraj (2015) and by Cai et al. (2014). In particular, according to Mohammed

* Corresponding author. Tel.: +39-011-090-6860.
E-mail address: giorgio.guglieri@polito.it

2352-1465 © 2018 The Authors. Published by Elsevier B.V.
This is an open access article under the CC BY-NC-ND license (https://creativecommons.org/licenses/by-nc-nd/4.0/)
Selection and peer-review under responsibility of the scientific committee of the International Conference on Air Transport – INAIR 2018.
10.1016/j.trpro.2018.12.006

et al. (2014) and Menouar et al. (2017), in the near future, UAVs will be used also in urban environments and they will be involved in the so-called smart cities.

Urban areas are a critical scenario, because they are inhabited environments. For this reason, the flight in urban areas is strongly limited by the National aviation agencies, such as ENAC (Ente Nazionale per l'Aviazione Civile) in Italy and the FAA (Federal Aviation Administration) in the United States. However, performing flight operations in cities is needed, thus a revision of aviation rules is mandatory for a full exploitation of aerial robotics in urban areas. As a consequence, flight operations over inhabited area must guarantee a certain level of safety, quantified by the risk assessment. A realistic and detailed risk assessment is one of the major challenges, since it is not easy to quantify the effective risk of a specific flight operation. There are a lot of factors involved, related to both the drone and the environment. This topic is discussed in Washington et al. (2017). In Clothier et al. (2018), the risk is modeled with a Barrier Bow Tie Model (BBTM) for risk analyses, evaluation and decision-making activities, in order to reduce the risk to people on ground. A real-time risk assessment framework is presented in Ancel et al. (2017), in order to perform real-time risk evaluation and tracking. A complete risk assessment process is described in Dalamagkidis et al. (2011), where the risk is defined as the probability to cause a casualty expressed in flight hour, a classic measure system used in the aviation for decades, as in FAA, Federal Aviation Administration (2000). This is a common approach, also used in Clothier et al. (2007), in la Cour-Harbo (2018) and in Guglieri and Ristorto (2016). The probabilistic risk assessment is often used to quantify the risk of a specific flight operation. In Bertrand et al. (2017), the authors quantify the risk for long-range inspection missions of railways.

In order to perform a safe flight operation, defining a safe path is mandatory. In Rudnick-Cohen et al. (2016) a risk-aware path planning is proposed, where a bi-objective optimization searches for a low risk and flight time solutions. In Primatesta et al. (2018) a risk-aware path planning based on dynamic risk-maps is proposed: first an offline optimal path is computed by trading off risk and path length, then, based on changes on the map, an online path planning algorithm adapts the path to maintain a safe and valid path. In Guglieri et al. (2015), an A* based algorithm minimizes the risk for flight operations. The risk-aware path planning is a common problem in robotics and it concerns also mobile robots in Feyzabadi and Carpin (2014), and underwater vehicles in Pereira et al. (2011).

In this paper an innovative algorithm able to compute an optimum risk path for UAVs in urban environments is proposed. First, a probabilistic risk assessment procedure is executed in order to generate a risk-map, *i.e.*, a map able to quantify the risk to the population over a specified urban area. Then, a risk-aware path planning algorithm seeks for the optimum risk path by minimizing the risk values taking into account the flight time. The basic principle of this approach is introduced in Primatesta et al. (2017), where a Cloud-based framework for the UAVs' risk-aware intelligent navigation in urban environments is introduced.

This paper is organized as follows. In Section 2, the proposed approach is introduced with its preliminary concepts. In Section 3 the risk-map is described in detail, focusing on the probabilistic risk assessment approach and introducing a new formulation to compute the area exposed to the crash. Section 4 defines the risk-aware path planning approach, while in Section 5 the simulation results are reported. Our conclusions are drawn in Section 6.

2. Proposed Method

In this section the proposed method to estimate risk optimum path is described. The procedure has two main phases: first, the risk-map is generated considering the vehicle parameters, thus, the path planner computes an optimal path considering the risk-map. The inputs of the risk-map generation are the drone parameters and the environment characteristics, such as the population density and the tridimensional model of the urban area. The resulting risk-map aims to quantify the risk relating the UAV on the population, defined as the frequency to have a casualty expressed in flight hour (h^{-1}). Hence, the risk-map is used to compute the minimum risk path. Since the risk depends on the flight time, the path planner seeks for an optimal path that minimizes the risk as a function of the flight time. The output of the path planner is a waypoint-based path able to be executed by the aircraft. In next sections the risk-map and the risk-aware path planner are described in detail.

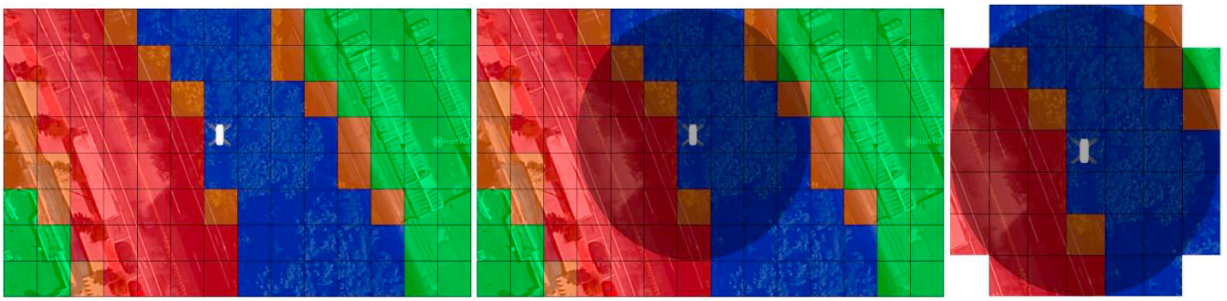

Fig. 1. From the left to the right: an example of general layer with UAV positioned on the analyzed cell; the hazardous area is computed considering the UAV position; only cells interested by the hazardous area are taken into consideration.

3. Risk-map

The risk-map is a two-dimensional georeferenced map divided into cells. For each of them, an on-population drone related risk value is associated. The risk-map is generated taking into account both the drone and the ground characteristics. The environmental data are stored into proper two-dimensional maps, called layers. In this work, the multilayer risk-map framework is composed by the following layers:

- **Obstacle Layer** defines the height of both fixed (buildings) and semi-static obstacles (construction sites) on the ground;
- **Population Density Layer** defines the population density;
- **Sheltering Factor Layer** defines the sheltering factor;
- **No Fly-zone Layer** defines the areas where the drone flight is not allowed.

All these layers are combined to generate the risk-map. First, with a probabilistic risk assessment approach, the cell risk-value is computed, taking into account the population density, the sheltering factor layer and the *hazardous area*, *i.e.*, the area interested by the descent of the UAV. Thus, it is merged with the obstacle and the sheltering factor layers with an element by element combination, obtaining the risk-map. This procedure is simple: each element of the risk-map $\mathbf{R}(i,j)$ has a value equal to -1 if it is a no-fly zone or if it is occupied by obstacles at the flight altitude, otherwise, it has the risk value associated to the risk-map element.

3.1. Hazardous Area

In the case of failure, the drone will probably roam several cells before to touch the ground. For this reason, when the risk of flying over a cell is computed, all the cells interested by the descent event are taken into account. These cells lie in an area, called *hazardous area*. Since the risk-map is generated before the definition of the flight operation, the direction of the aircraft is unknown. For this reason, the area is a circle with a radius defined by the maximum traveled distance of the UAV during the descent event. The hazardous area is defined based on the vehicle configuration type (Fig. 1).

3.1.1. Rotary wing aircraft

With the rotary wing aircraft, the following ballistic descent model is considered:

$$\begin{cases} \ddot{x} = -\frac{1}{2}\rho\dot{x}^2\frac{SC_D}{m} \\ \ddot{y} = -\frac{1}{2}\rho\dot{y}^2\frac{SC_D}{m} - \frac{g}{m} \end{cases}, \tag{1}$$

with m the mass of the vehicle, ρ is the air density, S is the vehicle frontal section and C_D is the related drag coefficient. x and y are the horizontal and vertical upward axis. Solving the Eq. 1, the maximum drone travelled distance is calculated, as well as the impact velocities.

3.1.2. Fixed wing aircraft

With the fixed wing aircraft, we consider the worst scenario, *i.e.*, the vehicle starts a descent as a glider with a known glide ratio ψ. The glide ratio defines the ratio between the traveled horizontal distance x_{dist} and the flight altitude h. Hence, $x_{dist} = \psi h$.

3.2. Risk Assessment

In this section, the method of merging information coming from the various layers in order to obtain the so-called risk-map is analyzed. The formulation used in this work is derived from a common probabilistic approach used in Dalamagkidis et al. (2011) and Clothier et al. (2007). Hence:

$$f_F = A_{exp} \cdot D_p \cdot P(\text{fatality}|\text{failure}) \cdot f_{GIA} , \tag{2}$$

where f_F is the casualty frequency: in this work, it represents the risk to the population on the ground. A_{exp} is the area exposed to the crash, referred to a single person. D_p is the population density. P(fatality|exposure) is the probability that a person will suffer fatal injuries given exposure to the accident. f_{GIA} is a rate of ground impact accidents.

The risk assessment formula is used to compute the risk value for each element of the map considering the hazardous area. This implies the use of the average value of population density in the hazardous area. Unlike the formulation at the state of the art, in this work different assumptions are considered on the sheltering factor and the area exposed to the crash.

3.2.1. Ground Impact Accidents Rate

The rate of ground impact accidents quantifies the frequency related to the loss the control of the UAV and the resulting impact to the ground. Often, it coincides with the failure rate of the aircraft system, expressed in flight hours. In Dalamagkidis et al. (2011), a constant value in the range [10^{-6} h^{-1}, 10^{-9} h^{-1}] is used. It comes from the average accident rate involving unmanned aircraft. However, the failure rate depends on the vehicle type and specifications: the higher the drone price, the lower it is. In la Cour-Harbo (2017), the author estimates the fatality rate of Micro Air Vehicles (MAV) using values of 0.5-10 h^{-1}. In Amos et al. (2013), the authors tried to estimate the failure rate of the Ultra Stick 120 aircraft with an average value of 2.16 failures per 100 flight hours.

3.2.2. Area Exposed to the crash

The area A_{exp}, also called *Casualty Area*, is the exposed area to the crash debris referred to a single person on the ground. In literature some methods to estimate it are proposed, as in Dalamagkidis et al. (2011). One of the most used formulation is presented in Smith (2000):

$$A_{exp}^{old}(\gamma) = 2\left(r_p + r_{uav}\right)\frac{h_p}{\tan(\gamma)} + \pi(r_p + r_{uav})^2 , \tag{3}$$

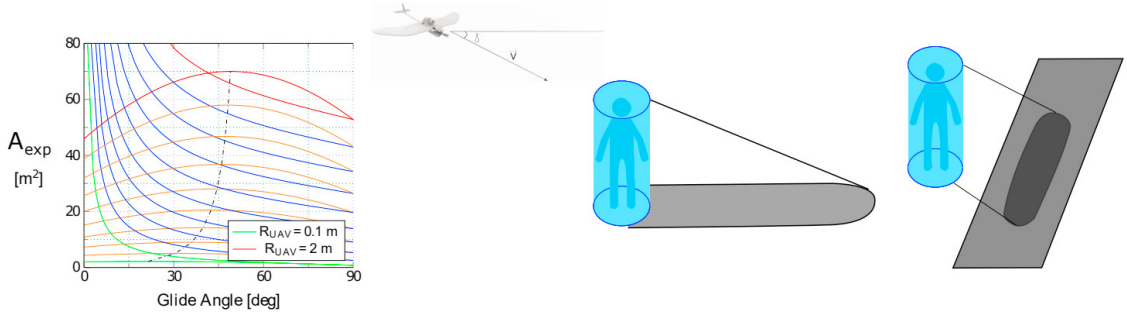

(a) (b) (c)

Fig. 2. In (a), the comparison between the old (blue line) and new (orange line) formulation considering different drone size. In (b), the representation of the exposed area with the old formulation proposed in Smith (2000). In (c), the representation of the new formula proposed in this work.

where γ is the glide angle, r_p and h_p are the radius and the height of cylinder idealizing an average person, and r_{uav} is the radius of the sphere containing the aircraft. In particular, r_{uav} is equal to the semi-wing span for fixed wing configuration, or a half of the maximum occupational length in rotary wing configuration. However, the Eq. (3) diverges when γ goes to zero. This happens because the formula is used for commercial space launch and reentry missions: it involves high kinetic energy, so the casualty area is overestimated for our purpose. The Eq. (3) is plotted in Fig. 2(a) (blue lines). In order to solve the above-mentioned problem, in this work a novel formulation is proposed. The hypothesis fulfilled are:

- The casualty area is very small compared to the area interested by the ground impact event;
- The casualty area consists in the all involved A_{exp}.

While in the old formula the exposed area is simply idealized as the man-cylinder shadow on the ground, in the proposed method the exposed area is the projection of the man-cylinder on a plane normal to the speed of the UAV. In fact, we consider that the UAV is offensive only for the first hit person. In Fig. 2(b) and Fig. 2(c), old and new methods are illustrated respectively.
Hence, the proposed method is defined by the following Equation:

$$A_{exp}^{new}(\gamma) = \pi\left(r_p + r_{uav}\right)^2 \sin(\gamma) + 2(r_p + r_{uav})(h_p + r_{uav})\cos(\gamma)\ . \tag{4}$$

The characteristics of the new formula, lead to new advantages. It is finite and has a maximum value (the dashed line in Fig. 2(a)): when the glide angle at impact is unknown, the maximum value can be used as casualty area.

3.2.3. Probability of fatality given exposure

The P(fatality|exposure) is the probability that the person hit by the aircraft suffers fatality injuries. Depending on the aircraft properties and on which part of body is affected, it is hard to estimate it. The available methods are the Blunt Criterion (BC) in Bir and Viano (2004) and the Viscous Criterion (VC) in Johannsen and Schindler (2005). They are based on the energy absorbed during the impact, but they are not suitable with low impact velocities. In this work, the method proposed in Dalamagkidis et al. (2011) is used:

$$P(fatality|exposure) = \frac{1-k}{1-2k+\sqrt{\frac{\alpha}{\beta}}\left[\frac{\beta}{E_{imp}}\right]^{\frac{3}{p_s}}}\ , \tag{5}$$

where $k = min\left[1, \left[\frac{\beta}{E_{imp}}\right]^{\frac{3}{p_s}}\right]$ is a correction factor. E_{imp} is the kinetic energy at the impact, p_s is the sheltering factor,

α is the impact energy required for a fatality of 50% when $p_s = 6$, and β is the impact energy threshold required to cause a fatality when p_s converges to zero. According to Dalamagkidis et al. (2011), acceptable values of α and β are 100 kJ and 34 J respectively. In the fixed wing aircraft case, the impact speed is 90% of the cruise speed, while in the rotary wings one, the impact velocity can be estimated by the ballistic descent model.
The sheltering factor quantifies how people on the ground are sheltered by buildings and obstacles. In Dalamagkidis et al. (2011), it lies in the range from 0 to +∞. According to Guglieri et al. (2014), it is useless to take into account high p_s values. In this work, the p_s belongs to the range from 0 to 10. In Table 1 is reported the sheltering factor criteria used in this work. Moreover, in order to evaluate all the cell interested by the descent of the UAV, the Eq. (5) uses the arithmetic mean value of the sheltering factor in the hazardous area.

Table 1. Sheltering Factor values.

Sheltering Factor	Typical Area
0	No obstacles
2.5	Sparse trees
5	Trees and low buildings
7.5	High buildings
10	Industrial area

4. Path planning

Once the risk-map is generated, the path planning aims to compute an optimal path minimizing the risk to the population according to the risk values in the risk-map.

In this work, a risk-aware path planning algorithm based on the well-known Optimal Rapidly-exploring Random Tree (RRT*) (Karaman and Frazzoli (2010)) is proposed. RRT* is an enhanced version of the original Rapidly-exploring Random Tree (RRT) proposed by LaValle (1998). RRT and RRT* are sample-based algorithms that explore the search space with an incremental tree. While RRT connects the new sampled state with the nearest one in the tree, the RRT* connects it to the branch with the minimum motion cost. Moreover, the rewiring procedure of RRT* optimizes the tree construction. Therefore, the RRT* algorithm converges to the optimal solution.

Since the risk values are expressed per flight hour, in this work we use the concept of *Time Reliance*: the probability of killing someone is proportional to how long the person is exposed to the risk. This assumption derives from the complex system failure probability calculation. During the useful life of the aircraft system, the probability to have a failure during a period of time t is equal to $P(E_{fail}) = t\rho$, with ρ is the failure rate during useful life phase (depending on the UAV) and t is the considered time. In our approach the failure rate of the vehicle is already considered in the risk assessment, as the rate to have a ground impact accident f_{GIA}. As a consequence, the proposed risk-aware path planner considers the risk in respect to the flight time.

Hence, the motion cost of the risk-aware RRT* is defined in the Eq. 6(a):

$$c_m(n_i) = c_m(n_{i-1}) + \int_{n_{i-1}}^{n_i} r(n)\, dt \quad \text{(a)}, \qquad c_m(n_i) = c_m(n_{i-1}) + \frac{r(n_{i-1})+r(n_i)}{2}\Delta t(n_{i-1}, n_i) \quad \text{(b)}, \quad (6)$$

where $c_m(n_{i-1})$ is the motion cost of the parent node n_{i-1}, $r(n)$ is the risk function defined by the risk values in the risk-map. Practically, because of the discrete search space (the risk map), the integral is computed with an approximative and incremental method, the Eq. 6(b), where $\Delta t(n_{i-1}, n_i)$ is the flight time expressed in hour needed to cover two adjacent nodes n_{i-1} and n_i.

5. Simulation results

The approach proposed in this paper is implemented in C++ as an executable process in ROS (Robot Operating System), an open-source meta-operating system for robots, presented in Quigley et al. (2009).

In particular, the risk-map is generated using the Grid Map library proposed in Fankhauser and Hutter (2016). Grid Map is a C++ library compatible with ROS that is able to generate two-dimensional grid maps with multiple data layers. The path planning is implemented using the Open Motion Planning Library (OMPL) in Şucan et al. (2012). OMPL is an open source library specialized in sampling-based motion planning and it consists of many state-of-the-art algorithms.

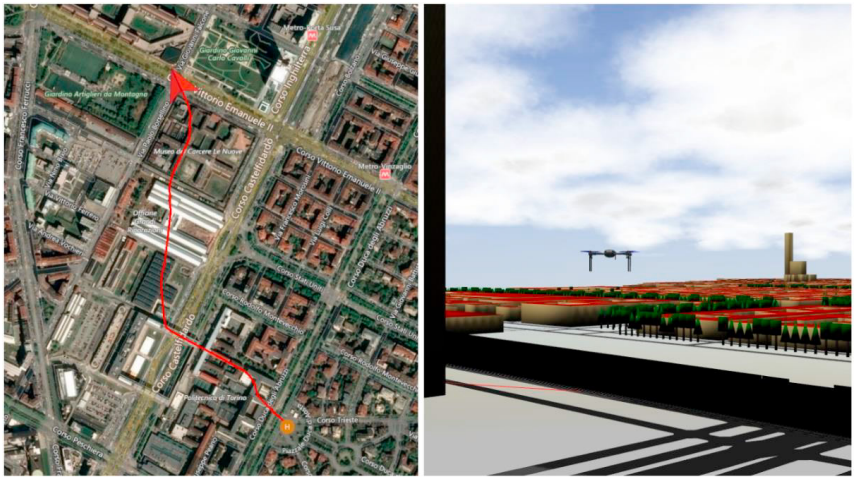

Fig. 3. On the left, the screen of the Ground Control Station (GCS), where the *Iris+* executes the minimum risk path with SITL simulator. On the right, the *Iris+* in the simulated environment in Gazebo

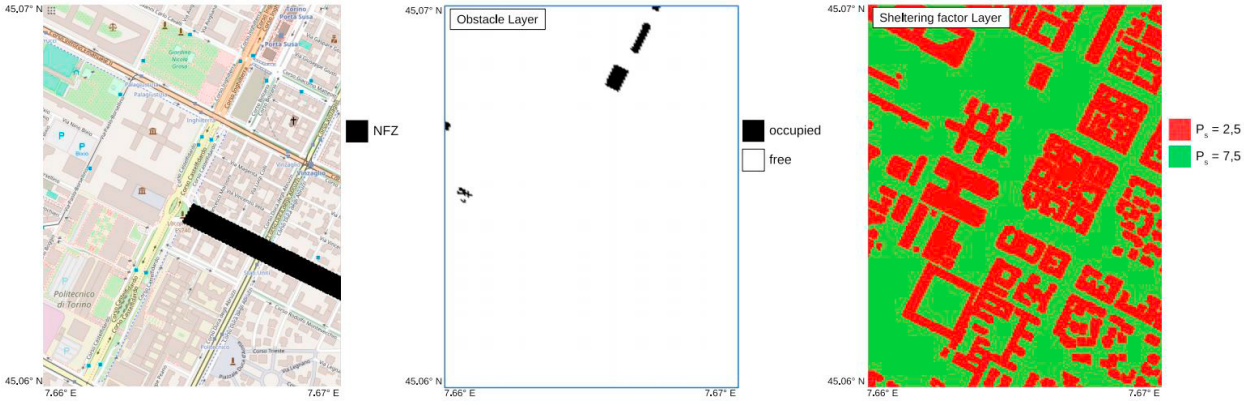

Fig. 4. From the left to the right: the map from OSM of the portion of city used to execute the simulation results, the obstacle layer and the sheltering factor layer. On the map of Turin is overlighted an imaginary no-fly zone.

In order to demonstrate the effectiveness of the risk-map and the path planning, the simulation results are obtained considering a portion of the city of Turin, Italy. The model of city is given by OpenStreetMap (OSM) OpenStreetMap contributors (2017), an open source project that distributes geographical data of the world. Thanks to it, the 3D model can be extracted, then, the obstacle layer is defined.

The proposed approach is also tested in a realistic simulation performed with SITL (Software In The Loop) SITL contributors (2017) and Gazebo simulator. SITL allows to simulate the autopilot of the vehicle, interfacing with a flight simulator, executing the control command and providing sensors data. The flight simulator is performed using Gazebo, a robot simulator compatible with ROS presented in Koenig and Howard (2004), while the *mavros* node

provides the communication between ROS and the autopilot, using the MAVLink protocol. Fig. 3 shows the simulation, where the *Iris+* executes an autonomous mission performing the minimum risk path reported in Fig. 5.

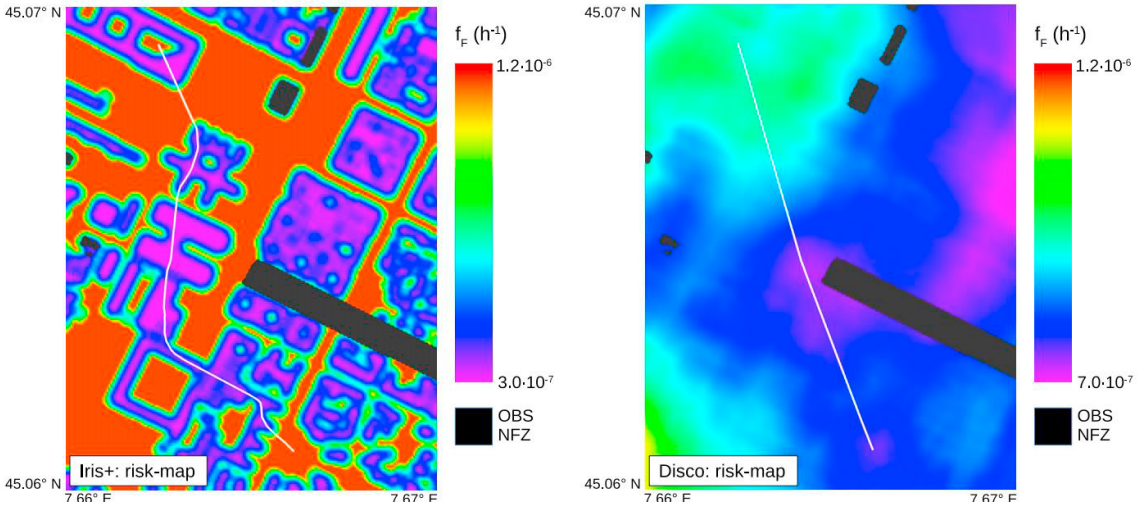

Fig. 5. On the left, the risk-map of the Iris+ aircraft. On the right, the risk-map of the Disco aircraft. Both maps are generated considering the flight altitude of 30 m. The white line is the minimum risk path computed with our risk-aware path planner.

The sheltering factor layer is determined with a simple method: a value of $p_s = 7.5$ is defined to the element occupied by buildings, whereas there is no information about the shelter, a value of $p_s = 2.5$ is set. The last one is an appropriate sheltering factor value, because the people in the street are often sheltered by trees, vehicles and low buildings. The population density layer is defined with a constant value of 6900 people/km^2, the population density of Turin.

In Fig. 4 is illustrated the portion of city from OSM, the obstacle layer at 30 m and the sheltering factor layer. Once all layers are defined, the risk-map can be generated. In order to demonstrate the proposed method, two aircraft are taken into consideration: the 3DRobotics *Iris+* and the Parrot *Disco*. These are two lightweight commercial drones, a quadrotor and a fixed wing aircraft, respectively. The drone specifications are reported in Table 2.

The risk-map is generated following the procedure described in this work and assuming a failure rate equals to 0.01 h^{-1}. The resulting maps computed with the both vehicles are illustrated in Fig. 5. The risk-maps differ each other, because of the different assumption about the vehicle configurations. Due to the smaller hazardous area, the conformation of the risk-map of the *Iris+* is strongly affected by the sheltering factor layer. In fact, the minimum risk is located over buildings, while the maximum risk over the opened areas, such as streets and parks.

On the contrary, the risk values in the risk-map associated to the Parrot *Disco* is uniformly distributed on the map. The main reason is the large hazardous area that implies mean values of sheltering in respect of the wide hazardous area.

The risk-map is now used to compute the minimum risk path. Given the same start and goal positions on the map, two paths are illustrated in Fig. 5, while the numerical results are reported in Table 3.

The risk-aware path planning algorithm produces interesting results. With the *Iris+* aircraft the minimum risk path passes over the rooftops of the buildings, because they are the area with the minimum risk. Differently, with the *Disco* aircraft the minimum risk path is practically a straight line. The main reason is the distribution of the risk. In the risk-map of the Parrot *Disco* the variation between the maximum and the minimum risk is small, as a consequence the path with the minimum risk in respect to the flight time is the shorter distance path.

In order to quantify the risk of a flight operation, it is important to evaluate the average risk of the flight mission. According to Dalamagkidis et al. (2011), an acceptable *Equivalent Level of Safety* (ELOS) is $1 \cdot 10^{-6}$ h^{-1}. In our test, the average risk is always lower than the ELOS threshold.

Since our risk-aware path planner minimizes the risk in respect to the flight time, it can decide to fly over a zone with high risk for few time. This happens with the *Iris+* aircraft, where the minimum risk path crosses an area with high risk in order to reach the goal position. However, the resulting average risk is acceptable.

Table 2. Specification of the aircraft.

Specific	3DR Iris+	Parrot Disco
Type	Quadrotor	Fixed wing
Mass (kg)	1.282	0.75
Radius (m)	0.35	0.575
Cruise speed (m/s)	10	12.5

Table 3. Results of the risk-aware path planning.

Vehicle	Solve time (s)	Flight time (s)	Path length (m)	Motion cost	Average risk (h^{-1})
Iris+	5.0	114.237	1142.372	$1.161 \cdot 10^{-8}$	$5.072 \cdot 10^{-7}$
Disco	5.0	80.544	1006.796	$1.883 \cdot 10^{-8}$	$8.416 \cdot 10^{-7}$

6. Conclusions

In this paper an innovative algorithm to compute an optimum risk path for unmanned aerial vehicle in urban environments is proposed. The risk-map is able to quantify the risk to the population of a large areas, considering the specification of a specified vehicle. It defines the risk level of each element and identifies the areas where the flight is not allowed because of the presence of obstacles at the flight altitude or no-fly zones forced by the National aviation agencies.

In order to define safe flight operations, the risk-map is used to compute a minimum risk path. In this paper it is proposed a path planning algorithm based on the well-known Optimal Rapidly-exploring Random Tree (RRT*) with the minimization of the risk values. Since the risk is expressed in flight hours, the path planner evaluates the risk in respect to the flight time. As a consequence, the path planning seeks for an optimal path by trading off the risk and the flight time.

The simulation results corroborate the proposed method. Results are obtained considering two vehicles with different specifications. The resulting risk-maps quantify the risk over the entire area and the path planning computes the minimum risk path.

The proposed approach is a very promising tool, because it is able to define safe flight operations. Especially in urban environments, where the public safety is the most important element.

Future works include the improvement of the risk assessment, considering different descent events and a more realistic model. Also, the path planning can be improved considering kinodynamic constraints and the adaptation to tridimensional environments.

Acknowledgements

This work was supported by a fellowship from TIM, by the Siebel Energy Institute, by Compagnia di San Paolo, and by MIT-Italy MITOR seed grant.

References

Amos, J., Bergquist, E., Cole, J., Phillips, J., Reimann, S., Shuster, S., 2013. UAV for Reliability. Technical Report. University of Minnesota, Minneapolis, MN.

Ancel, E., Capristan, F.M., Foster, J.V., Condotta, R.C., 2017. Real-time risk assessment framework for unmanned aircraft system (UAS) traffic management (UTM), in: 17th AIAA Aviation Technology, Integration, and Operations Conference, p. 3273.

Bertrand, S., Raballand, N., Viguier, F., Muller, F., 2017. Ground risk assessment for long-range inspection missions of railways by uavs, in: Unmanned Aircraft Systems (ICUAS), 2017 International Conference on, IEEE. pp. 1343–1351.

Bir, C., Viano, D.C., 2004. Design and injury assessment criteria for blunt ballistic impacts. Journal of Trauma and Acute Care Surgery 57, 1218-1224.

Cai, G., Dias, J., Seneviratne, L., 2014. A survey of small-scale unmanned aerial vehicles: Recent advances and future development trends. Unmanned Systems 2, 175–199.

Chmaj, G., Selvaraj, H., 2015. Distributed processing applications for uav/drones: a survey, in: Progress in Systems Engineering. Springer, pp. 449–454.

Clothier, R.A., Walker, R.A., Fulton, N., Campbell, D.A., 2007. A casualty risk analysis for unmanned aerial system (uas) operations over inhabited areas, in: AIAC12, Twelfth Australian International Aerospace Congress, 2nd Australasian Unmanned Air Vehicles Conference, pp. 1–15.

Clothier, R.A., Williams, B.P., Hayhurst, K.J., 2018. Modelling the risks remotely piloted aircraft pose to people on the ground. Safety science 101, 33–47.

la Cour-Harbo, A., 2017. Mass threshold for 'harmless' drones. International Journal of Micro Air Vehicles 9, 77–92.

la Cour-Harbo, A., 2018. Quantifying ground impact fatality rate for small unmanned aircraft. Journal of Intelligent & Robotic Systems, 1–18. doi:10.1007/s10846-018-0853-1.

Dalamagkidis, K., Valavanis, K.P., Piegl, L.A., 2011. On integrating unmanned aircraft systems into the national airspace system: issues, challenges, operational restrictions, certification, and recommendations. volume 54. springer science & Business Media.

FAA, Federal Aviation Administration, 2000. System safety handbook. Department of transportation, Washington DC, USA.

Fankhauser, P., Hutter, M., 2016. A Universal Grid Map Library: Implementation and Use Case for Rough Terrain Navigation, in: Koubaa, A. (Ed.), Robot Operating System (ROS) – The Complete Reference (Volume 1). Springer. chapter 5. doi:10.1007/978-3-319-26054-9_5.

Feyzabadi, S., Carpin, S., 2014. Risk-aware path planning using hierarchical constrained markov decision processes, in: Automation Science and Engineering (CASE), 2014 IEEE International Conference on, IEEE. pp. 297–303.

Guglieri, G., Lombardi, A., Ristorto, G., 2015. Operation oriented path planning strategies for rpas. American Journal of Science and Technology 2, 1–8.

Guglieri, G., Quagliotti, F., Ristorto, G., 2014. Operational issues and assessment of risk for light uavs. Journal of Unmanned Vehicle Systems 2, 119–129.

Guglieri, G., Ristorto, G., 2016. Safety assessment for light remotely piloted aircraft systems, in: INAIR 2016, International Conference on Air Transport, pp. 1–7.

Johannsen, H., Schindler, V., 2005. Review of the abdomen injury criteria. Technical Report. Institut National de Reserche sur les Transports et leur Sécurité, Tech. Rep. AP-SP51-0039-B.

Karaman, S., Frazzoli, E., 2010. Incremental sampling-based algorithms for optimal motion planning. Robotics Science and Systems VI 104, 2.

Koenig, N., Howard, A., 2004. Design and use paradigms for gazebo, an open-source multi-robot simulator, in: 2004 IEEE/RSJ International Conference on Intelligent Robots and Systems (IROS), pp. 2149–2154. doi:10.1109/IROS.2004.1389727.

LaValle, S.M., 1998. Rapidly-exploring random trees: A new tool for path planning. TR 98-11, Computer Science Dept., Iowa State University.

Menouar, H., Guvenc, I., Akkaya, K., Uluagac, A.S., Kadri, A., Tuncer, A., 2017. Uav-enabled intelligent transportation systems for the smart city: Applications and challenges. IEEE Communications Magazine 55, 22–28.

Mohammed, F., Idries, A., Mohamed, N., Al-Jaroodi, J., Jawhar, I., 2014. Uavs for smart cities: Opportunities and challenges, in: Unmanned Aircraft Systems (ICUAS), 2014 International Conference on, IEEE. pp. 267–273.

OpenStreetMap contributors, 2017. Planet dump retrieved from https://planet.osm.org. https://www.openstreetmap.org.

Pereira, A.A., Binney, J., Jones, B.H., Ragan, M., Sukhatme, G.S., 2011. Toward risk aware mission planning for autonomous underwater vehicles, in: Intelligent Robots and Systems (IROS), 2011 IEEE/RSJ International Conference on, IEEE. pp. 3147–3153.

Primatesta, S., Capello, E., Antonini, R., Gaspardone, M., Guglieri, G., Rizzo, A., 2017. A cloud-based framework for risk-aware intelligent navigation in urban environments, in: Unmanned Aircraft Systems (ICUAS), 2017 International Conference on, IEEE. pp. 447–455.

Primatesta, S., Guglieri, G., Rizzo, A., 2018. A risk-aware path planning strategy for uavs in urban environments. Journal of Intelligent & Robotic Systems, 1–15. doi:10.1007/s10846-018-0924-3.

Quigley, M., Conley, K., Gerkey, B., Faust, J., Foote, T., Leibs, J., Wheeler, R., Ng, A.Y., 2009. Ros: an open-source robot operating system, in: ICRA workshop on open source software, p. 5.

Rudnick-Cohen, E., Herrmann, J.W., Azarm, S., 2016. Risk-based path planning optimization methods for unmanned aerial vehicles over inhabited areas. Journal of Computing and Information Science in Engineering 16, 021004.

SITL contributors, 2017. SITL guide retrieved from https://planet.osm.org. http://ardupilot.org/dev/docs/ sitl-simulator-software-in-the-loop.html.

Smith, P.G., 2000. Expected Casualty Calculations For Commercial Space Launch and Reentry Missions - Advisory Circular. Technical Report.

Şucan, I.A., Moll, M., Kavraki, L.E., 2012. The Open Motion Planning Library. IEEE Robotics & Automation Magazine 19, 72–82. doi: 10.1109/MRA.2012.2205651.

Washington, A., Clothier, R.A., Silva, J., 2017. A review of unmanned aircraft system ground risk models. Progress in Aerospace Sciences 95.